Synthesis of NIR/SWIR Absorbing InSb Nanocrystals Using Indium(I) Halide and Aminostibine Precursors

Yongju Kwon, Oleksandra Yeromina, Mariarosa Cavallo, Mathieu G Silly, Debora Pierucci, Emmanuel Lhuillier, Dmitry Aldakov, Bérangère Hyot, Peter Reiss

ADVANCED FUNCTIONAL MATERIALS
www.afm-journal.de

Synthesis of NIR/SWIR Absorbing InSb Nanocrystals Using Indium(I) Halide and Aminostibine Precursors

*Yongju Kwon, Oleksandra Yeromina, Mariarosa Cavallo, Mathieu G. Silly, Debora Pierucci, Emmanuel Lhuillier, Dmitry Aldakov, Bérangère Hyot, and Peter Reiss**

Colloidal InSb quantum dots (QDs) are a potential alternative to toxic Pb- and Hg-chalcogenide QDs for covering the technologically important near-infrared/shortwave infrared (NIR/SWIR) spectral range. However, appropriate Sb precursors are scarce and obtaining narrow size distributions is challenging. Tris(dimethylamido)antimony ($Sb(NMe_2)_3$) is an appealing choice due to its commercial availability and non-pyrophoric character but implies the reduction of antimony from the +3 to the required –3 state. In reported works, strong reducing agents such as lithium triethylborohydride are used, which lead to the fast co-reduction of both Sb^{3+} and In^{3+}. The downsides of this approach are reproducibility issues and the risk of forming metal nanoparticles due to the different reduction kinetics of Sb^{3+} and In^{3+}. Here, indium(I) halides are explored as simultaneous indium source and mild reducing agent for the antimony precursor. The wavelength of the excitonic absorption peak of the phase-pure InSb QDs obtained with this approach can be tuned from 630 to 1890 nm, which corresponds to a size range of ≈2–7 nm. The synthesis can also be conducted in a heat-up manner, which facilitates the scale-up and paves the way for the use of InSb QDs in applications such as NIR/SWIR photodetectors, cameras, biological imaging, and telecommunications.

1. Introduction

Narrow bandgap colloidal quantum dots (QDs) offer exceptional promises for low-cost infrared active applications combining many advantages such as tunable absorption and fluorescence emission spectra, high molar extinction coefficients, high photoluminescence (PL) quantum yield, high stability, cost-efficient and scalable synthesis, and solution processability.[1] One of the advantages of using infrared radiation stems from reduced Rayleigh scattering of light in the air at longer wavelengths, induced for example by dust or fog. By consequence, short wavelength infrared (SWIR: 1–2.5 µm) cameras can "see" through haze better than visible-range cameras.[2] Also, the use of near-infrared (NIR: 0.7–1 µm) light enables much larger penetration depths in biological tissues to perform deep-tissue imaging. In the NIR-I (650–900 nm) and NIR-II/SWIR (1000–1700 nm) windows, tissues have low scattering, absorption, and autofluorescence background.[3] Other useful applications of colloidal IR QDs have been explored in photovoltaics, infrared light-emitting diodes (LEDs), telecommunication, solar concentrators, thermoelectric devices, and optical sensing.[4] Most of the reported NIR and/or SWIR active QDs are based on materials containing toxic heavy metals, such as PbS and HgTe QDs.[2a,5] A(III)-B(V) semiconductors containing one group-13 and one group-15 element of the periodic table are highly promising Pb- and Hg-free alternative materials.

Colloidal indium antimonide (InSb) QDs have been considered a low-toxic alternative to Pb or Hg chalcogenide QDs in the NIR/SWIR spectral regions. Bulk InSb possesses a narrow direct bandgap (0.17 eV at 300 K), high static dielectric constant

Y. Kwon, O. Yeromina, D. Aldakov, P. Reiss
Univ. Grenoble Alpes
CEA
CNRS
Grenoble INP
IRIG
SyMMES
17 rue des Martyrs, Grenoble 38000, France
E-mail: peter.reiss@cea.fr

The ORCID identification number(s) for the author(s) of this article can be found under https://doi.org/10.1002/adfm.202403912

DOI: 10.1002/adfm.202403912

M. Cavallo, D. Pierucci, E. Lhuillier
Sorbonne Université
CNRS
Institut des NanoSciences de Paris
4 Place Jussieu, Paris 75005, France

M. G. Silly
Synchrotron SOLEIL
L'Orme des Merisiers
Départementale 128, Saint-Aubin 91190, France

B. Hyot
Univ. Grenoble Alpes
CEA
Leti
17 rue des Martyrs, Grenoble 38000, France

($\epsilon = 17$), the highest room temperature electron mobility (7.7×10^4 cm^2 V^{-1} s^{-1}), lowest thermal conductivity (0.18 W $cm^{-1}K^{-1}$), and smallest exciton binding energy (0.5 meV) of all common semiconductors.[6] This latter feature, lost in many other "greener" alternatives to toxic heavy metal-based QDs, is of particular interest for photodetection as electrons and holes almost behave like free charges. Also, due to the large exciton Bohr radius of InSb (≈60 nm),[7] the bandgap energy of InSb QDs can be tuned in a broad range throughout the NIR and SWIR spectrum through size control, as a consequence of quantum confinement. Given the inherent advantages of colloidal synthesis methods (which are generally economic and scalable), this approach enables the use of colloidal InSb QDs as building blocks in low-cost, solution-processed optoelectronic devices, such as field-effect transistors, photodetectors, thermoelectric devices, LEDs, and solar cells.

Despite these promises, only very few chemical synthesis methods for colloidal InSb QDs have been reported, which is mainly due to the limited choice of suitable pnictogen precursors. In 2008, the formation of colloidal InSb QDs was reported using indium stearate and tris(trimethylsilyl)antimony ($(TMS)_3Sb$) as precursors.[8] The $(TMS)_3Sb$ precursor is an analog of $(TMS)_3As$ and $(TMS)_3P$ which have been commonly used for syntheses of InAs or InP QDs. These tris(trimethylsilyl)pnictogenide chemicals are highly reactive to form III-V semiconductor QDs but they are also highly pyrophoric, air- and moisture-sensitive, and of limited commercial availability. Also, the high reactivity of $(TMS)_3Sb$ makes it hard to control the nucleation and growth processes of InSb QDs and leads to a broad size distribution.[8] Therefore, the obtained absorption spectrum is featureless, i.e., no excitonic peak is visible. In situ formed SbH_3 has been tried as an alternative precursor for the synthesis of InSb QDs.[9] However, the synthesized InSb QDs showed once again a featureless absorption spectrum and no size tuning was possible. In the quest for safer and easier use of group V precursors giving access to high-quality InSb QDs, tris(di(trimethylsilyl))amide stibine ($Sb[N(SiMe_3)_2]_3$),[10] antimony chloride ($SbCl_3$)[11] or tris(dimethylamido)antimony ($Sb(NMe_2)_3$)[12] have been explored more recently. Unlike the $(TMS)_3Sb$ or SbH_3 precursors that exhibit −3 oxidation state for Sb, antimony in $Sb[N(SiMe_3)_2]_3$, $SbCl_3$ and $Sb(NMe_2)_3$ is in its +3 oxidation state, making the precursors more stable. On the other hand, additional reducing agents are required in these reactions such as lithium triethylborohydride ($LiEt_3BH$),[10,11,12b,d,13] lithium di(trimethylsilyl)amide ($Li[N(SiMe_3)_2]$),[12b] *n*-butyllithium (*n*-BuLi),[12b,c] or alane *N*,*N*-dimethylethylamine (DMEDA).[14] Their use leads to the co-reduction of the antimony and indium precursors and the formation of Sb(0) and In(0) species which rapidly form InSb nuclei.[12b,13c] However, the use of highly reactive reducing agents negatively impacts reproducibility, bears the risk of generating metallic side-products, and makes it challenging to control nucleation and growth in the InSb QDs synthesis. As a result, the InSb QDs formed using these pathways generally show broad excitonic absorption features and post-synthetic size fractionation is required, e.g., using size-selective precipitation.[10,12,13] Therefore, it is highly desirable to explore other ways of reducing aminostibine precursors in the synthesis of InSb QDs, giving direct access to narrow size distributions and enabling the tuning of their absorption spectra in a wide NIR/SWIR range.

In this study, we report a novel synthesis method for colloidal NIR/SWIR-active InSb QDs using In(I)X (X = Cl, Br, I) and $Sb(NMe_2)_3$ precursors without the addition of a strong reducing agent. In this reaction scheme, In(I)X plays the dual role of indium source and mild reducing agent for the antimony precursor being itself oxidized to the required In(III) state. In(I) halides have been recently proposed in the synthesis of InP and InAs QDs using amino-pnictogen group V precursors,[15,16] however, the reaction behavior differs markedly from the case of InSb. Here, InSb QDs with well-defined excitonic absorption peaks are synthesized at a comparably low temperature of 230 °C using In(I)Br or In(I)I in combination with $Sb(NMe_2)_3$. In contrast, In(I)Cl leads to broad absorption features indicative of a much larger size distribution. The wavelength of the excitonic absorption peak of the InSb QDs could be tuned in an unprecedentedly large range from 630 to 1890 nm by adjusting the reaction parameters such as the halide type, reaction temperature, and time. The minimum excitonic peak linewidth of the as-prepared QDs is 200 meV (full width at half maximum, FWHM), while the PL peak width is 150 meV demonstrating narrow size distribution without any size-selective purification. From a mechanistic point of view, NMR studies demonstrate that the premixing step of the In and Sb precursors likely induces the formation of In–Sb intermediates prior to QD nucleation at high temperature. This step is of crucial importance for obtaining high-quality, phase-pure nanocrystals without any metallic (In^0, Sb^0) or oxide (In_2O_3) side-products after purification. Finally, we show that the proposed synthesis method can be used also in a heat-up manner, i.e., without precursor injection into the hot solvent, which facilitates its scale-up to larger quantities.

2. Results and Discussion

2.1. Synthesis of InSb QDs and Wavelength Tuning of the Absorption Properties

A standard synthesis following the procedure developed here consists of two steps. First, In(I)X and $Sb(NMe_2)_3$ are premixed in oleylamine (OAm) and reacted at 50 °C for 1 h. In terms of size distribution, the best precursor molar ratio between In(I)X and $Sb(NMe_2)_3$ turned out to be 6:1 for In(I)Cl or In(I)Br and 3:1 for In(I)I; the effect of this ratio will be discussed in more details later. The color of the premixed InSb precursor solution turns brown immediately when the temperature reaches 50 °C and no more solid residue is visible with In(I)I. The obtained solution is quickly injected into 1-octadecene (ODE) solvent at 230 °C containing trio-*n*-octylphosphine (TOP, 4 eq. based on $Sb(NMe_2)_3$). Details of the experimental procedure and control experiments can be found in the Methods section. UV-vis-NIR absorption spectra were recorded for different reaction times and varying the indium halide precursor (**Figure 1**). Figure 1a shows the absorption spectra of InSb QDs synthesized from In(I)Cl and $Sb(NMe_2)_3$. A broad absorption feature with an FHWM of 537 meV appeared at 1094 nm after 10 min, which redshifted to 1280 nm after 60 min. The peak energies and FWHM were determined using Gaussian fitting (cf. Figure S1, Supporting Information).

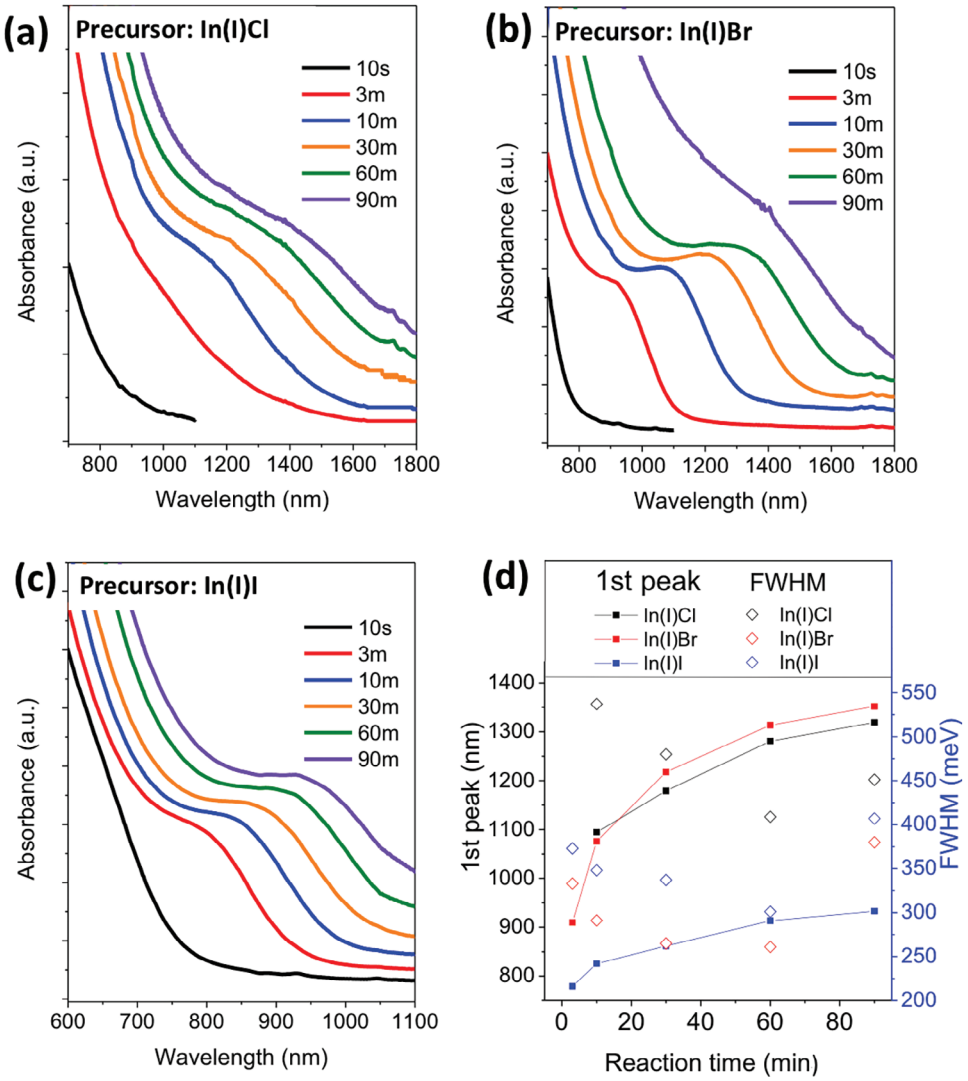

Figure 1. Indium halide dependence of the absorption properties. UV–vis-NIR absorption spectra of aliquots taken over time during the synthesis of InSb QDs from a) In(I)Cl, b) In(I)Br, and c) In(I)I reacted with $Sb(NMe_2)_3$ at 230 °C in ODE. The In:Sb precursor ratio is 6:1 for In(I)Cl and In(I)Br, 3:1 for In(I)I. d) Evolution of the excitonic absorption peak position (full symbols) and its linewidth (FWHM, hollow symbols) as a function of the reaction time for the 3 indium precursors.

Compared to In(I)Cl, the In(I)Br and In(I)I precursors resulted in better-defined excitonic absorption features (Figure 1b,c). When In(I)Br was reacted with $Sb(NMe_2)_3$ at 230 °C, the absorption peak shifted from 910 to 1352 nm as the reaction proceeded from 3 to 90 min (cf. Figure 1b; Table S1, Supporting Information). During the first 60 min, the FWHM decreased from 333 to 261 meV showing size-focusing and indicating a diffusion-controlled growth mode. However, for longer times (90 min), only a weak shoulder is visible in the absorption spectrum characteristic of the broadening of the size distribution. It is induced by the decrease of the monomer concentration which becomes too low to maintain homogeneous particle growth from solution and leads to a ripening-type growth regime. In(I)I resulted in shorter wavelengths compared to In(I)Br covering a range of 780 to 933 nm (Figure 1c). This behavior can be attributed to the difference in reactivity of the In(I)X precursors. The bond dissociation energies for In–Cl, In–Br, and In–I are 439, 418, and 331 kJ mol^{-1}, respectively. The weaker In(I)–I bond is easier to dissociate, favoring the formation of a larger number of nuclei and resulting in smaller final QD sizes. Furthermore, the halides are involved in the surface passivation of the InSb QDs as confirmed by elemental analysis (vide infra). Due to the higher steric demand of the larger iodide ions compared to bromide, the surface-reaction and hence growth rates are reduced resulting in smaller particle sizes. In our recent study, we observed a similar behavior by varying the halide type of In(I)X precursors in the case of InP QDs.[16] In(I)Cl resulted in larger-sized, tetrahedral InP QDs with edge lengths >10 nm, while In(I)I precursor yielded much smaller sized InP QDs of ≈5 nm. In the present InSb synthesis, In(I)Cl does not follow the same tendency: it results in QDs with a similar excitonic absorption peak position as with the In(I)Br precursor (cf. Figure 1a,b). However, due to

the very broad linewidth of the absorption feature, it can be concluded that the In(I)Cl precursor is less suitable for the synthesis of InSb QDs of narrow size distribution using the present method. When the premixed InSb precursor solution was prepared using In(I)Cl and $Sb(NMe_2)_3$ in OAm, we observed a significant amount of In(0) metal precipitated at 50 °C after 1 h unlike the cases of In(I)Br and In(I)I (Figure S2, Supporting Information) indicating that In(I)Cl preferentially forms In(0) via the disproportionation reaction between In(I) and In(0)/In(III)[15] and/or the reduction of In(I) by OAm. For this reason, in the following, we will focus on the use of In(I)Br and In(I)I rather than In(I)Cl. As mentioned above, using these precursors, the absorption peak position could be tuned from 780 to 1352 nm at 230 °C. To shift the absorption onset further to the larger wavelength SWIR range, higher reaction temperatures of 260 and 280 °C were explored with In(I)Br; for comparison, the reactions were also performed with In(I)I (**Figure 2**). Using In(I)Br, at 260 °C the absorption peaks could be controlled from 1140 to 1760 nm with a FWHM of 230–280 meV (Figure 2a). Raising the reaction temperature further to 280 °C, the growth finishes quickly in 10 min resulting in a wavelength of 1732 nm for the final sample with a comparably narrow FWHM of 200 meV (Figure 2b); for longer reaction times at this temperature precipitation occurred.

Increasing the reaction temperature induced faster growth kinetics and resulted in a red-shift of the absorption peaks of the InSb QDs (Figure 2c) for both In(I)Br and In(I)I. While the wavelength could be tuned from 780 to 933 nm at 230 °C for In(I)I (Figure 1c), a range of 865–1160 nm (FWHM: 230–436 meV was achieved at 260 °C (Figure 2d). At 280 °C, a further red-shift occurred to 890 – 1250 nm, albeit with a broadening of the spectral features (FWHM 348–441 meV) (Figure 2e,f). As expected from the results at 230 °C (Figure 1), In(I)Br led in comparison with In(I)I to longer wavelengths of the excitonic absorption peak. 260 °C turned out to be the ideal temperature in that case, yielding the largest wavelength tunability (≈1100–1760 nm) while keeping a comparably narrow FWHM (cf. Figure 2a-c). Table S1 (Supporting Information) gives an overview of the influence of the reaction time, temperature, and type of indium halide on the excitonic peak position and linewidth.

Switching from the hot-injection method to the heat-up method corresponds to a significant simplification of the synthesis process, generally improving its reproducibility and scalability.[17] Here, we compare the results obtained with both methods using In(I)Br and In(I)I precursors (**Figure 3**). In the heat-up process, the premixed InSb precursor solution is injected into ODE solvent with TOP at room temperature and the resulting mixture is then heated to 230 °C with a rate of 20–30 °C min^{-1}. Compared with the hot-injection method, this heat-up synthesis resulted in a wider range of wavelength tunability of the excitonic absorption peaks. For the In(I)Br precursor, it could be varied from 730 to 1480 nm using the heat-up synthesis with a target temperature of 230 °C (Figure 3a), while the hot-injection synthesis resulted in a range of 910–1315 nm (Figure 1b). In the case of In(I)I, the values are 630–940 nm for the heat-up synthesis (Figure 3b) and 780–915 nm for hot-injection (Figure 1c). Considering the linewidth, the peaks get narrower in the early stage of the heat-up reaction, with a minimum just when the reaction temperature of 230 °C is reached, during the subsequent growth they broaden due to ripening (Figure 3c). On the contrary, in the hot-injection approach, as discussed before a narrowing of the peaks is observed up to 60 min (Figure 3d), while broadening occurs for longer reaction times (Figure 1d). Summarizing the results of both types of reactions, the excitonic absorption peaks of InSb QDs could be tuned from in a broad range of 630 to 1760 nm by adjusting the reaction parameters such as the halide precursor types (In(I)Br or In(I)I), reaction temperature, and reaction times. The wavelength range can be further extended from 1765 to 1880 nm by a secondary precursor addition using a solution containing In(I)Br and $Sb(NMe_2)_3$ (Figure S3a,b, Supporting Information). The obtained InSb QDs have weak photoluminescence (PL) intensity (PLQY < 1%). As a representative example, the PL spectrum of a sample obtained at 230 °C with In(I)Br PL is given in Figure 2h. The PL peak has an FWHM of 150 meV at 1315 nm indicating a narrow size distribution and exhibits a Stokes shift of 170 meV. The PL spectrum of another sample emitting ≈1500 nm is given in Figure S3c (Supporting Information). To increase the PLQY, the surface passivation via the growth of shell(s) of appropriate wider bandgap materials would an obvious option. In the case of InSb, InP appears as an appealing candidate to act as an intermediate shell between the InSb core and Zn-chalcogenide outer shells due to the type I band alignment and absence of toxic elements.

2.2. Structural Analyses of the InSb QDs

Transmission electron microscopy (TEM) analyses were performed to determine the size and size distribution of the QDs. The smallest InSb nanocrystals obtained with the In(I)I precursor in the hot-injection synthesis exhibiting an excitonic absorption peak at 780 nm have an average diameter of 2.0±0.35 nm (Figure S4, Supporting Information). Overall, the size of the InSb QDs could be tuned from ≈2 to 7 nm (**Figure 4**) by varying the reaction conditions. Size distributions of ≈15% were obtained for the as-synthesized QDs, i.e., without any size fractionation procedure such as size-selective precipitation.

The composition of the QDs was analyzed using EDS. For a representative sample obtained with In(I)Br showing an excitonic absorption peak at 1314 nm (mean size 3.9 nm), the composition was found as 1.15:1 (In:Sb). This ratio indicates the presence of an indium-rich surface (Table S2, Supporting Information). At the same time, the atomic ratio of In to Br is 1:0.37 demonstrating that Br^- ligands play an important role in the surface passivation, compensating for the charge neutrality of the InSb QDs. When using the In(I)I precursor, the In-to-halide ratio is lower (1:0.14) due to the larger steric demand of iodide ions. Co-passivation with halides has also been observed in other III-V QDs prepared from $InCl_3$ and aminopnictogen precursors.[18]

Analysis of the obtained InSb QDs has been further conducted using energy-tunable high-resolution X-ray photoemission spectroscopy (XPS). Using synchrotron radiation, we are able to tune the incident photon energy and the associated escape depth of the emitted photoelectrons. Laboratory experiments are generally conducted with a high energy source operated at 1253 eV (Mg source) or 1486 eV (Al source), which corresponds to an escape depth of a few nm. Therefore, in the case of small nanocrystals, using these energies can actually correspond to bulk analysis. Here, using lower incident photon energy, we can obtain more

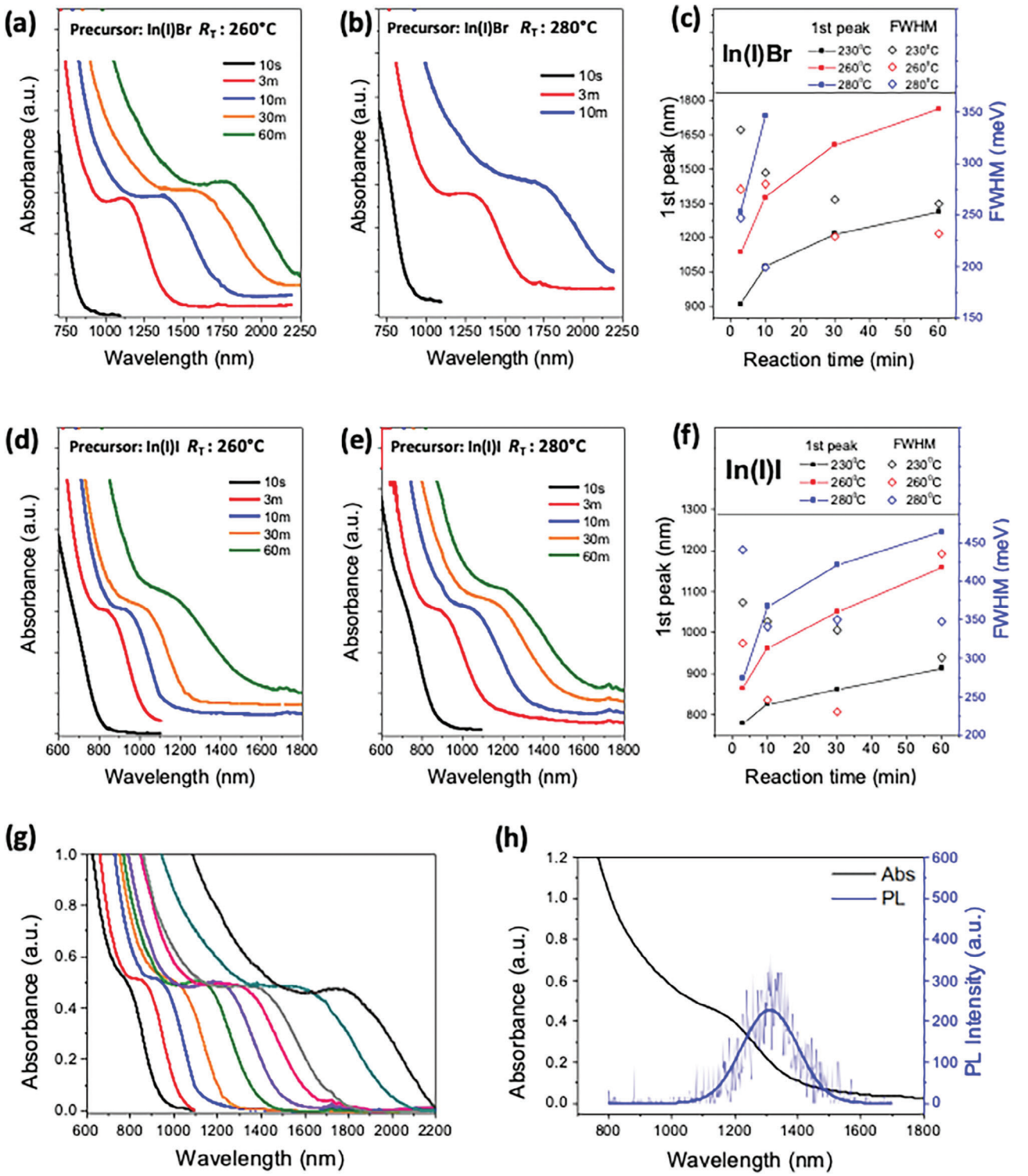

Figure 2. Temperature dependence of the absorption properties. UV-vis-NIR absorption spectra of aliquots taken over time during the syntheses of InSb QDs from In(I)Br and $Sb(NMe_2)_3$ at a) 260 °C and b) 280 °C. c) Evolution of the 1st excitonic absorption peak position (full symbols) and its linewidth (FWHM, hollow symbols). The same series of samples have been acquired with In(I)I and $Sb(NMe_2)_3$ at d) 260 °C and e) 280 °C; f) depicts the corresponding excitonic peak positions (full symbols) and linewidth (hollow symbols). g) Overview of the achievable wavelength tunability of the absorption spectra using the different reaction parameters discussed. From left to right the samples were prepared using the following conditions: (1) InI, 230 °C, 3 min; (2) InI, 230 °C, 30 min; (3) InI, 260 °C, 10 min; (4) InI, 260 °C, 30 min; (5) InBr, 230 °C, 3 min; (6) InBr, 230 °C, 30 min; (7) InBr, 230 °C, 60 min; (8) InBr, 260 °C, 10 min; (9) InBr, 260 °C, 30 min; (10) InBr, 260 °C, 60 min. h) Absorption and photoluminescence spectra of InSb QDs obtained by reaction of In(I)Br and $Sb(NMe_2)_3$ at 230 °C for 60 min.

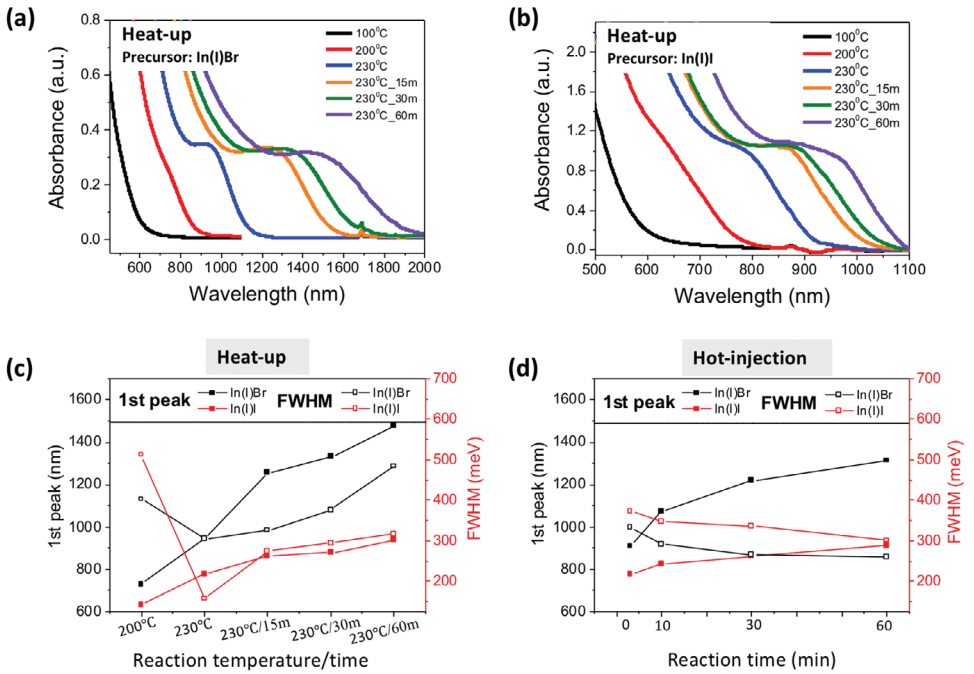

Figure 3. Heat-up synthesis of InSb QDs. UV-vis-NIR absorption spectra of aliquots taken over time during the syntheses of InSb QDs from a) In(I)Br and b) In(I)I and $Sb(NMe_2)_3$. Evolution of the excitonic absorption peak position (full symbols) and its linewidth (FWHM, hollow symbols) of InSb QDs obtained with c) the heat-up and d) the hot-injection method (230 °C).

surface-sensitive conditions and genuinely unveil the nature of the QD surface. A survey XPS spectrum is shown in **Figure** 5a. In addition to features arising from In and Sb, we also notice the presence of states associated with carbon and nitrogen that we can directly associate with the capping oleylamine ligands. Bromide is also detected, which comes from the used indium precursor (In(I)Br), and co-passivates the surface as discussed above. Despite rigorous air-free preparation and minimized post-synthetic exposure of the samples to air (i.e., the time to introduce the sample in the photoemission load-lock chamber), there is evidence of oxidation with a peak at 532.1 eV associated with the O 1s state. This energy range also overlaps with that from the Sb 3d

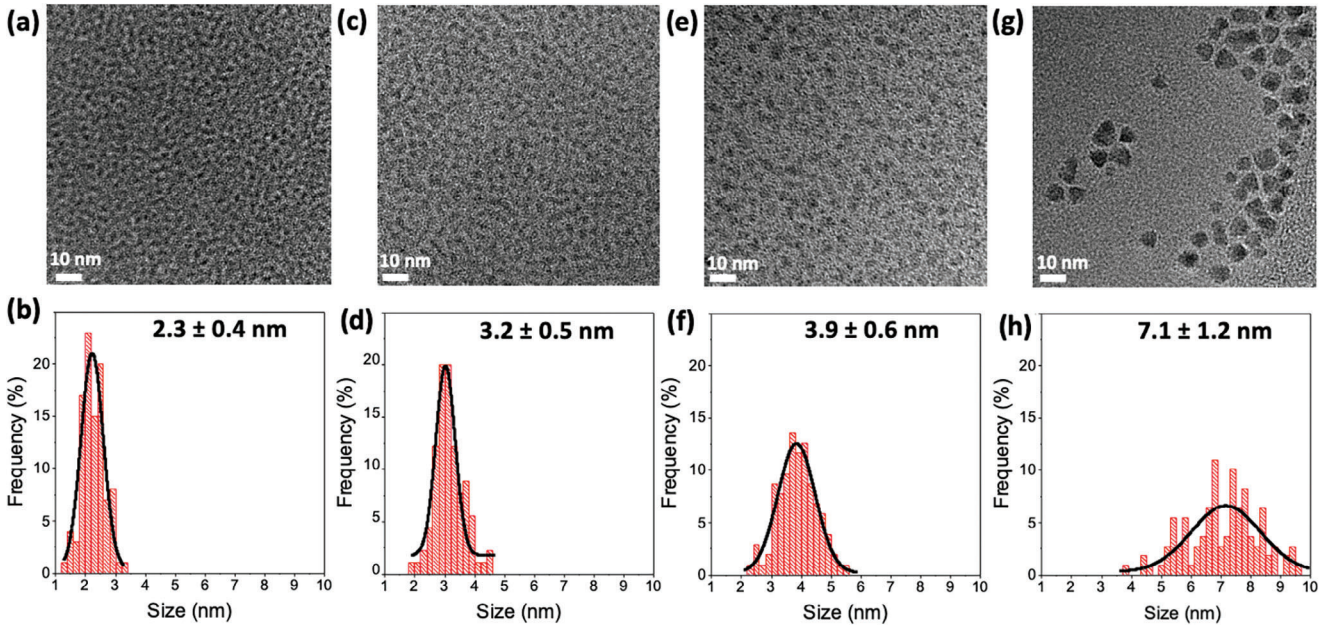

Figure 4. TEM analyses. TEM images and size histograms of InSb QDs obtained a, b) with In(I)I after 10 min, c, d) after 60 min at 230 °C; e, f) with In(I)Br after 60 min at 230 °C, and g, h) with In(I)Br after 30 min at 280 °C.

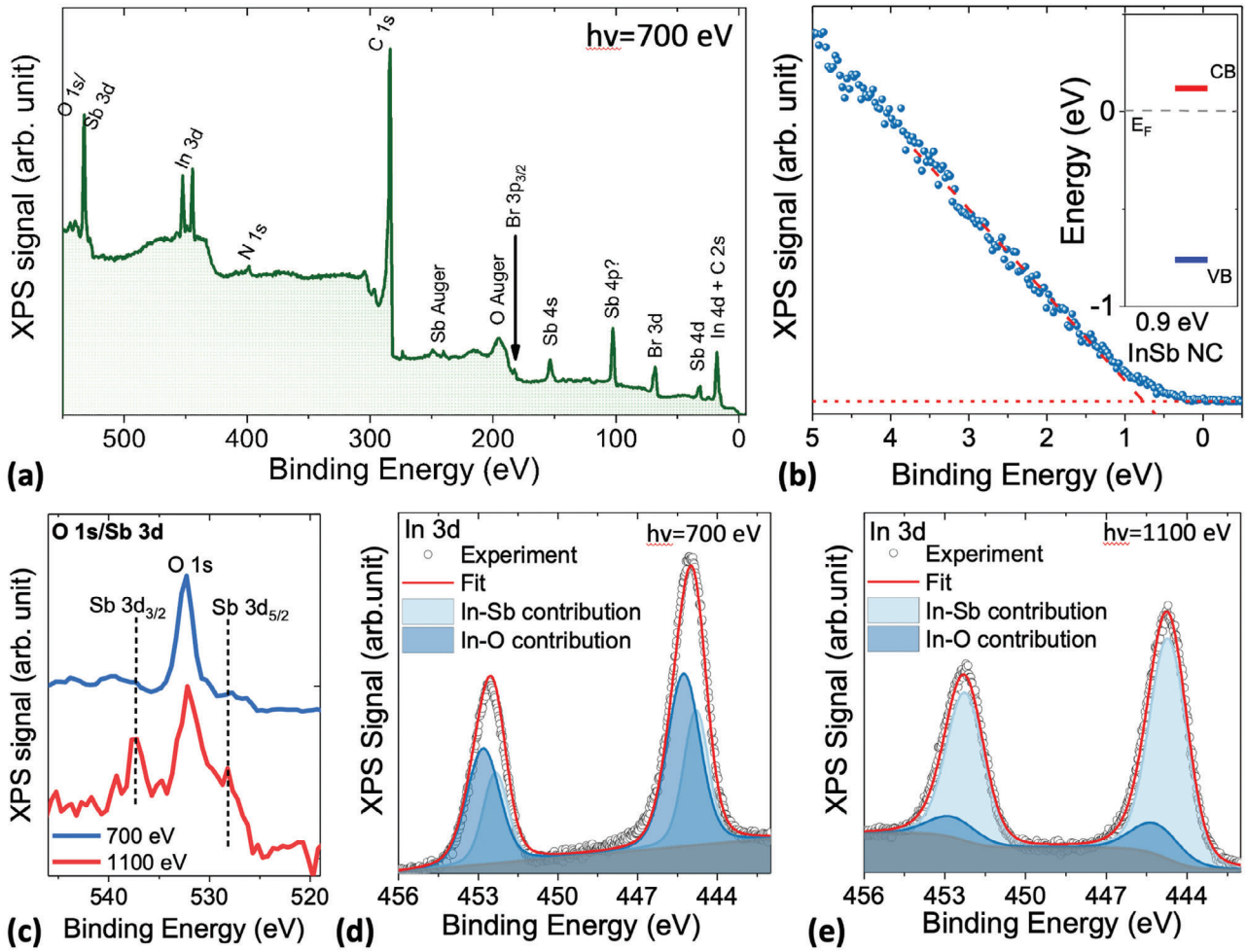

Figure 5. XPS analyses. Photoemission characterization of InSb nanocrystals with 0.9 eV band gap (InBr, 230 °C, 60 min). a) Survey spectrum acquired at 700 eV photon energy. b) Valence band spectrum acquired a 150 eV photon energy. Inset is a reconstructed energy diagram assuming a 0.9 eV band gap and neglecting any Coulombic term. c) O 1s and Sb 3s state acquired using 700 eV (surface sensitive conditions) and 1100 eV (bulk sensitive conditions) photon energies. d)/(e) In 3d state photoemission spectrum acquired at 700 eV/1100 eV.

state; however, we cannot detect the latter at low photon energy, suggesting that the surface is, in accordance with the EDS results, Sb-deficient (cf. Figure 5c). Further indications of the structure are obtained by observing the In 3d state that includes two contributions, one at 444.8 eV characteristic of In bound to Sb, and a second one at a higher binding energy of 445.2 eV, associated with In oxide due to the higher electronegativity of oxygen compared to Sb.[12b,19] The relative weight of these two contributions dramatically changes with the incident photon energy. The oxide contribution is stronger at low energy (i.e., surface sensitive condition), strongly reduced as the photon energy increases, and might be missed by the usual laboratory instrument. In the bulk, indium is essentially fully coordinated by Sb. Concluding, the QD exhibits a core/shell structure with an InSb core surrounded by an indium oxide shell. Investigation of the valence band signal (Figure 5b) reveals a valence band localized 0.76 eV below the Fermi level. Given the 0.9 eV band gap of these NC obtained from absorption spectroscopy, and neglecting the exciton binding energy given the large dielectric value of InSb (ϵ_r ranging from 10 to 100 depending on confinement and doping) we can reconstruct an effective electronic structure (inset of Figure 5b), which corresponds to a Fermi level in the upper part of the band gap suggesting an n-type behavior for this material. What remains to be elucidated is whether this behavior is an intrinsic property of InSb QDs or if the doped indium oxide shell (similarly to ITO) tends to induce it.[20]

2.3. Further Factors Influencing the Size and Size Distribution

Among further parameters potentially affecting the size and size distribution of InSb QDs, the precursor stoichiometry, i.e., the In(I)X: $Sb(NMe_2)_3$ ratio, deserves special attention. In principle, three equivalents of In(I)X are required because each In(I) ion can transfer two electrons to reduce Sb from the +3 state in aminostibine to the −3 state in InSb. However, higher ratios of In(I)X, in particular 6 equivalents of In(I)Cl or In(I)Br, resulted in narrower size distributions and higher chemical yields of the

reactions (Figure S5, Supporting Information). In contrast, with In(I)I the best defined absorption spectra was obtained with an In:Sb precursor ratio of 3:1. However, the use of these conditions also led to the formation of a small fraction of In(0) nanoparticles of ≈20 nm size as visible from TEM analyses (Figure S6, Supporting Information). As a consequence, the EDS data of InSb QDs obtained from In(I)I shows an indium-rich composition (In: Sb = 1.8) because of the presence of a mixture of InSb QDs and In(0) nanoparticles (Table S2, Supporting Information), and the X-ray diffractogram exhibits features of amorphous In(0) nanoparticles (or their oxidation products) as visible in Figure S7c (Supporting Information). Lowering the In: Sb precursor stoichiometry from 3:1 to 3:2 allowed preventing from In(0) formation leading to phase-pure InSb QDs, albeit at the cost of the size distribution: their absorption spectra are featureless without any excitonic peak (Figure S7a,b, Supporting Information).

Furthermore, the overall concentration of precursors has some influence on the evolution of the size distribution. When doubling the concentrations from 40 mM of In(I)I and 13 mM of $Sb(NMe_2)_3$ to 80 mM and 26 mM, respectively, (Figure S8a,b, Supporting Information), ripening at the end of the growth stage can be reduced as visible from the decreased linewidth after 90 min, while maintaining the same evolution of the absorption peak position (Figure S8c, Supporting Information).

Next, the influence of the solvent was studied, comparing OAm and ODE in the suitable temperature range of 230–280 °C. With OAm, higher and lower temperatures were also explored using In(I)I: at 210 °C, only a ripening-type growth yielding very broad absorption features was observed (Figure S9a, Supporting Information), while the temperature range between 230 and 280 °C turned out most suitable to form InSb QDs of narrow size distribution, as for the case with ODE solvent (Figure S9b-d, Supporting Information). At 320 °C, reaction products precipitate right from the beginning, possibly due to fast reduction following the formation of metallic side-products (Figure S9e, Supporting Information). It should be noted that OAm is ubiquitously used as the solvent in the synthesis of InP and InAs QDs using aminopnictogen precursors, and also in the majority of recent works on InSb QDs.[13] However, as mentioned above, with ODE the linewidth gets narrower from 333 to 261 meV as the reaction proceeded from 3 to 60 min (InBr, 230 °C), indicative of size-focusing via a diffusion-controlled growth mode. On the opposite, using OAm under the same conditions leads to a broadening of the absorption peak from 301 to 416 meV, attributed to ripening-type growth of the InSb QDs (Figure S10, Supporting Information). Broader absorption peaks and increasing linewidth over reaction time with OAm were also observed at higher temperatures (280 °C) or when using In(I)I instead of In(I)Br (Figure S11, Supporting Information). In addition, the use of OAm generally gives rise to shorter wavelengths of the excitonic peak than ODE. These differences can be attributed to the coordinating character of OAm, which strongly modifies the reaction kinetics. With OAm, there is only one set of parameters (InI, 230 °C) yielding QDs of similar quality as with ODE; under these conditions, the reaction kinetics, excitonic peak positions, and linewidths are quasi-identical to the ODE case (cf. Figure S11e, Supporting Information). At higher temperatures (280 °C), with OAm the particle shape evolves toward various bi-, tri-, and tetrapods of homogeneous arm thickness and variable arm length (Figure S11f, Supporting Information). Summarizing, ODE appears as the better choice of solvent than OAm for the synthesis of InSb QDs starting from In(I) halide and aminostibine precursors.

Finally, the influence of trioctylphosphine (TOP) addition was studied. TOP is not found in the final product according to our EDS, XPS, and NMR data, however, it acts as an important reaction additive modulating the reactivity of the indium precursor and enabling narrow size distribution of the as-synthesized InSb QDs (Figure S12, Supporting Information). In our optimized conditions, we use 4 equivalents of TOP per $Sb(NMe_2)_3$ and in the absence of TOP, the absorption peak gets much broader (Figure S12a,b, Supporting Information). On the other hand, adding more than 4 equivalents does not lead to further improvement (Figure S12c, Supporting Information).

The minimum value of FWHM is obtained as 200 meV from In(I)Br precursors (Figure 2b,c) and 165 meV from In(I)I in the heat-up approach (Figure 3b,c) confirming the narrow size distribution obtained with this synthesis method in comparison with reported ones. Most of the time the spectra are given after performing size-selective precipitation to narrow down the size distribution.[10,12d] Here, In(I)Br and In(I) act as mild reducing agents for $Sb(NMe_2)_3$ making diffusion-controlled growth of the InSb QDs possible from monomers in solution. When highly reactive species such as superhydride are used as the reducing agents, the fast kinetics leads to a rapid depletion of the monomer reservoir, and the InSb QDs grow further by ripening and/or aggregation, which leads to broader, sometimes even bimodal size distributions.[12d] On the contrary, the use of the In(I) halides provides a robust and reproducible synthetic pathway, allowing for facile size tuning of the InSb QDs by changing the reaction parameters such as the halide type, reaction temperature, or reaction time. We found that the best parameters are to use of In(I)Br and $Sb(NMe_2)_3$ in a 6:1 ratio, reacted at 260 °C with the presence of 4 equivalents of TOP per $Sb(NMe_2)_3$ in ODE solvent. When In(I)I is applied, the In:Sb ratio should be 3:1 and the temperature lower, e.g., 230 °C, to obtain InSb QDs of narrow size distribution.

2.4. Effect of the In and Sb Precursors Premixing Stage

The redox chemistry involved in the aminostibine approach may lead to the formation of side-products such as metallic In(0) and Sb(0), eventually induced by OAm acting as a reducing agent for the In(I)X and $Sb(NMe_2)_3$ precursors. This behavior can indeed be seen when the precursors are heated individually in OAm, i.e., without premixing, as confirmed by X-ray diffraction analysis. In(I)X precursors heated without the Sb precursor in OAm at 50 °C for 1 h generate crystalline In(0) particles (Figure S13a, Supporting Information). $Sb(NMe_2)_3$, in turn, is reduced by OAm to Sb(0) (which then oxidizes to Sb_2O_3) at 230 °C, i.e., the reaction temperature for the synthesis of the InSb QDs (Figure S13b, Supporting Information). Already from these observations can be concluded that the premixing of In(I)X and $Sb(NMe_2)_3$ before heating to the reaction temperature is a critical step to get phase-pure InSb QDs. **Figure 6** gives further confirmation of this hypothesis by comparing two identical syntheses with and without the premixing step. The product obtained with premixing

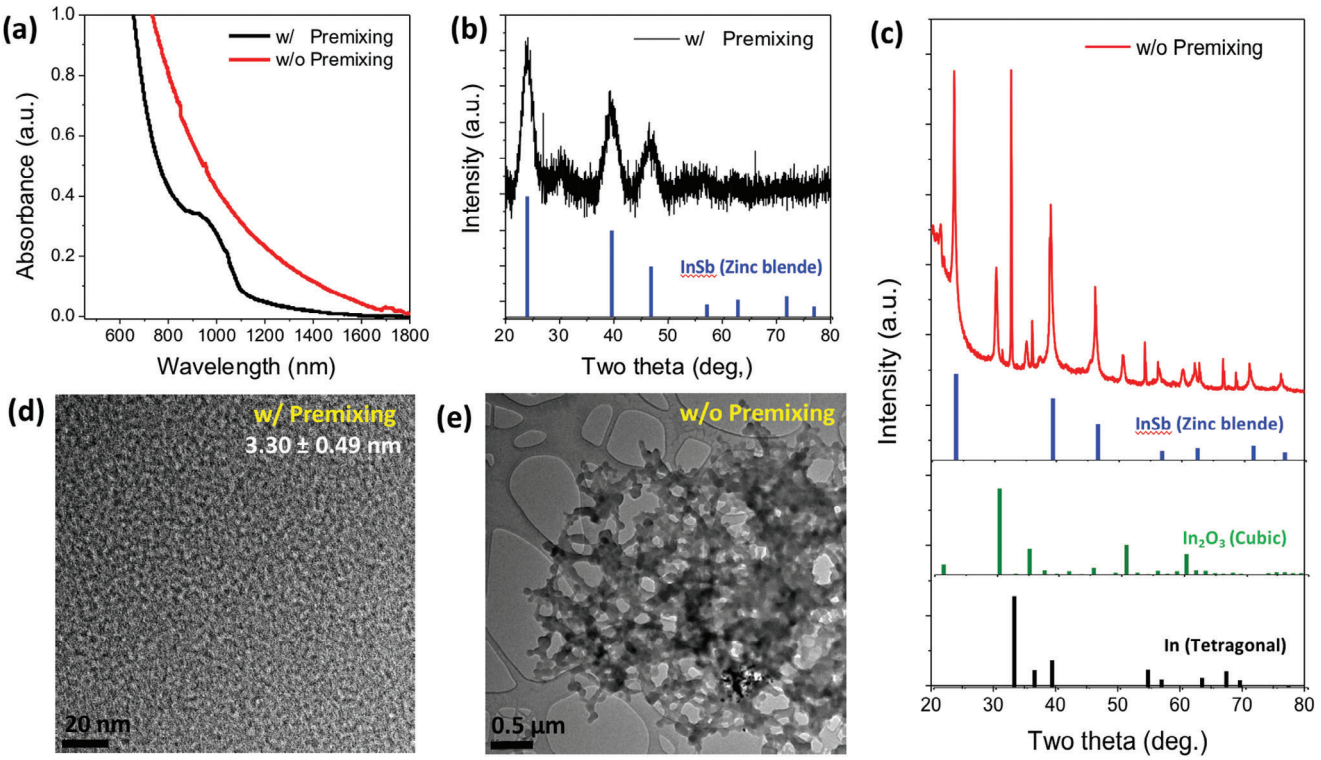

Figure 6. Influence of the In and Sb precursors premixing stage. a) Vis-NIR absorption spectra of the reaction products obtained with (black line) or without (red line) premixing the precursors (In(I)Br and $Sb(NMe_2)_3$) for 1 h at 50 °C prior to their injection into a mixture of OAm and TOP at 230 °C (reaction time: 10 min). XRD patterns of syntheses obtained b) with premixing, c) without premixing. The reference diffraction patterns of bulk InSb, In_2O_3, and In(0) are also given for comparison. TEM images of the synthesis products obtained d) with premixing, e) without premixing.

exhibits an excitonic absorption peak near 1000 nm characteristic for InSb QDs features and the XRD pattern corresponds to the cubic zinc blende phase of InSb. A small contribution of In_2O_3 at around 30° (2 theta) is visible, which is attributed to surface oxidation occurring during the measurement (Figure 6a,b). Using the Scherrer equation, a small crystallite size of 3.4 nm was calculated, which is at the origin of the broad linewidths observed in the diffractogram. To study the effect of the premixing step, in a second experiment the $Sb(NMe_2)_3$ solution in OAm was directly injected into an In(I)Br solution in OAm/TOP at 230 °C. The obtained product exhibits a featureless absorption spectrum and the XRD pattern revealed a mixture of InSb, metallic In(0), and In_2O_3 (Figure 6a,c). The peaks corresponding to InSb display narrow linewidths corresponding to nanoparticles of ≈25 nm. Also, In(0) formed as a side-product which then presumably oxidized to In_2O_3 during the purification and/or the X-ray data acquisition. TEM images of the products demonstrate that with the premixing step, homogeneous InSb QDs are obtained with an average diameter of 3.3 nm (Figure 6d), in good accordance with the crystallite size determined from XRD. Without premixing, on the other hand, inhomogeneous and large-sized products are observed which form extended aggregates (Figure 6e). These aggregates may form during the melting of metallic In(0) nanoparticles; the melting temperature of bulk indium is 230 °C.

Starting from $In(III)Cl_3$, Busatto et al. recently reported a similar trend with a premixing step of the In and Sb precursors being mandatory to avoid the formation of metallic side products.[12d] More precisely, $In(III)Cl_3$ and $Sb(NMe_2)_3$ were mixed with OAm and toluene at room temperature, and then the obtained InSb precursor solution was injected into OAm at high temperature (240 °C) after the addition of $LiEt_3BH$. Supported by NMR studies, the formation of a pre-bond between In(III) and Sb(III) was proposed to occur during the premixing step.

To analyze the InSb precursor solution in our case, we selected In(I)I due to the absence of any visible precipitate, while precursor solutions involving In(I)Br and In(I)Cl contain a small fraction of precipitated metallic indium. First of all, we optimized the experimental conditions of the premixing step by varying the reaction temperature, mixing time, and solvent (Figure S14, Supporting Information). Premixing the precursors at 50 °C for 1 h leads to InSb QDs with narrow size distribution (Figure S14a, Supporting Information), while there is no excitonic absorption feature if the premixing step is shortened to 10 min (Figure S14b, Supporting Information). When performing the premixing step at lower temperature (25 °C), dissolution of the precursors is still possible when the mixing time is increased to 2h30. However, the InSb QDs obtained from this mixture start to precipitate after a growth time of ≈30 min at 230 °C. Moreover, their diffraction patterns exhibit peaks characteristic of metallic Sb and In_2O_3 products (Figure S14c,d, Supporting Information), while no peaks corresponding to the InSb QDs are visible. This is a strong evidence that 25 °C is too low to induce the formation of the precursor complex presumably containing the preformed In–Sb bond, which is

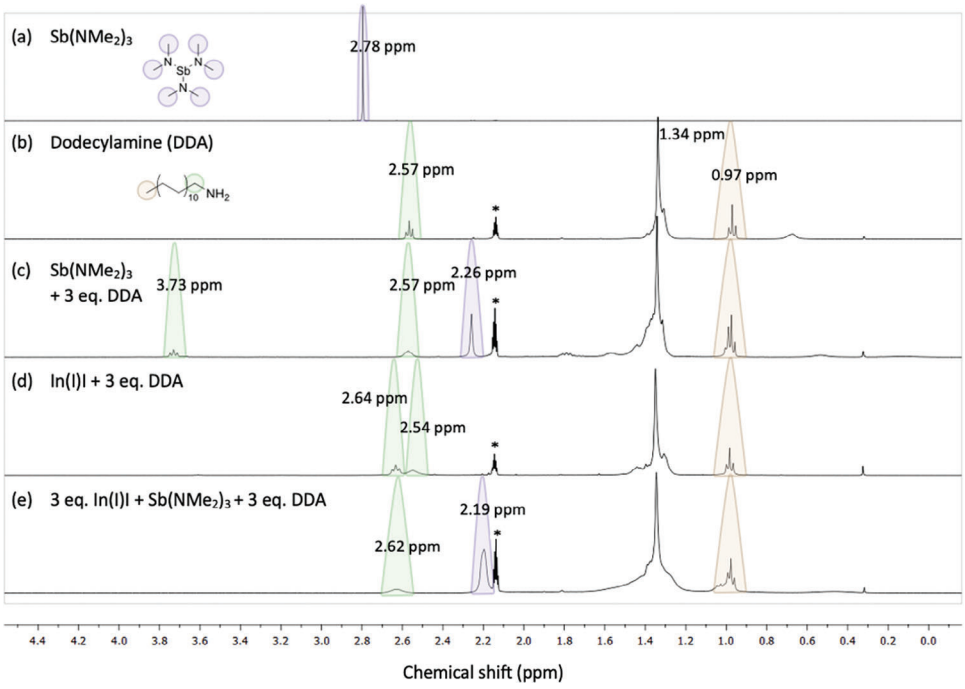

Figure 7. ^{1}H-NMR analyses of the premixed InSb precursor solution containing In(I)I, $Sb(NMe_2)_3$, and DDA. ^{1}H-NMR spectra of a) $Sb(NMe_2)_3$, b) DDA, c) $Sb(NMe_2)_3$ with 3 eq. of DDA, d) In(I)I with 3 eq. of DDA, and e) 3 equiv. of In(I)I, 1 equiv. of $Sb(NMe_2)_3$ and 3 equiv. of DDA in toluene-d8, heated to 50 °C for 1 h. The asterisk (*) indicates the toluene signal.

required for the formation of InSb QDs. Finally, the solvent for the premixing step was changed from OAm to ODE, while keeping at 3 eq. of OAm to achieve the transamination. We observed that ODE dissolved the In(I)I precursor much slower as it does not act as a Lewis base unlike OAm. By consequence, it took 4h30 at 50 °C to obtain a clear solution. However, once again precipitation of the products after ≈20 min of growth at 230 °C was seen (cf. Figure S14e, Supporting Information), in this case probably induced by the insufficient amount of surface-capping OAm ligands.

For further analysis, we first tried to isolate the precursor complex obtained with the optimized conditions by precipitation. Premixing In(I)I and $Sb(NMe_2)_3$ (3:1) in OAm at 50 °C for 1 h, yields a dark-brown solution that displays a featureless absorption spectrum in the Vis-NIR spectral range below 2000 nm (Figure S15a, Supporting Information). Precipitation was induced by the addition of anhydrous methanol and acetone (1 vol.eq. of each) inside a glove box. EDS data showed that the precipitate is mostly composed of In and that the Sb fraction is extremely low even when considering the used 3:1 In:Sb ratio (Figure S15b, Supporting Information). XRD analysis revealed the amorphous character of the product with broad signals in the region of the peaks characteristic for the tetragonal In(0) and cubic In_2O_3 phases (Figure S15c, Supporting Information). TEM and SEM images exhibited aggregated particles with an average diameter of 135 nm (Figure S15d, Supporting Information). We hypothesize that the precipitation with the polar solvents induces the formation of In(0) particles, which partially oxidize during the sample preparation for TEM and XRD. Therefore, this precipitation procedure is not appropriate to study the expected mixed In–Sb precursor complex.

To get more insight in the species present in the liquid state after the premixing stage, ^{1}H-NMR experiments were performed (**Figure 7**). Instead of OAm, we used dodecylamine (DDA) because of its higher purity, and we confirmed in preliminary experiments that DDA does not alter the spectra of the QDs, even though a slightly broader size distribution is obtained (Figure S16a,b, Supporting Information). The ^{1}H NMR spectrum of $Sb(NMe_2)_3$ in toluene-d8 displays one peak, a singlet at 2.78 ppm, which corresponds to the methyl protons of $-N(CH_3)_2$ (Figure 7a). The spectrum of DDA, $CH_3(CH_2)_{11}NH_2$, has four distinct peaks, a broad signal at 0.68 ppm from the –NH group, a triplet at 0.97 ppm from the terminal methyl group $-CH_3$, a multiplet centered at 1.34 ppm from $-CH_2-$ of the alkyl chain, and a triplet at 2.57 ppm related to $-N(CH_2)-$ protons (Figure 7b). Once $Sb(NMe_2)_3$ is mixed with 3 equivalents of DDA, two new peaks appeared, a singlet at 2.26 ppm and a triplet at 3.73 ppm (Figure 7c). The singlet corresponds to methyl protons of dimethylamine (DMA), $(CH_3)_2NH$, which is formed during the transamination reaction between $Sb(NMe_2)_3$ and DDA leading to $Sb_x[(CH_3)_2N]_{3-y}[CH_3(CH_2)_{11}NH]_y$.[12d] This transamination reaction is well known for the aminopnictogen precursors.[12d,15,16,21] Pure DMA has a singlet peak at 2.18 ppm in deuterated toluene,[12d] while the peak attributed to DMA formed in our sample is slightly deshielded to 2.26 ppm. The triplet at 3.75 ppm is assigned to $-N(CH_2)-$ from DDA bound to Sb. The observed downfield shift compared to the signal of free DDA (2.57 ppm) is due to the coordination to the metal site.[22] Meanwhile, a fraction of free DDA remained present, as a broad peak at 2.57 ppm was observed. This indicates that less than 3 DDA molecules interact with one Sb center (Figure 7c). Integrating the peaks of free DDA (2.57 ppm), bound DDA (3.73 ppm), and

total DDA (0.97 ppm) results in a molar ratio of 1.3:1:2.4, showing the peak assignments are reliable and resulting in an average value of 1.3 DDA per Sb. Not reaching 3 DDA molecules per Sb center can be expected in the present conditions due to the insufficient excess of primary amine. In mechanistic studies on InP QDs synthesis using aminophosphine precursors and In(I) or In(III), for low oleylamine:aminophosphine ratios (e.g., <10), oleylimido-bridged or heterocyclic species have been detected in addition to the triply transaminated aminophosphine.[16,21a]

Next, we analyzed the ^{1}H-NMR spectrum of the mixture of In(I)I with 3 equivalents of DDA, yielding a dark-brown precipitate probably caused by a limited solubility of In(I) salts in amines at low temperatures. Moreover, because of the disproportionation equilibrium of the indium(I) precursor, In(I)I, In(III)I_3, and In(0) coexist in the In(I)I-DDA solution, and as In(0) has the propensity to form nanoparticles (Figure 6e), which tend to precipitate with time, the solution becomes turbid (**cf**. Figure S16c, Supporting Information). Consequently, three types of In-DDA can be formed such as In(I)I$(DDA)_x$, In(III)$I_3(DDA)_y$, and DDA bound to In(0) particle surfaces. In the ^{1}H-NMR spectrum of the obtained suspension, a triplet at 2.64 ppm and a broad signal at 2.54 ppm are observed (Figure 7d). The peak broadening of the –N(CH_2)– is attributed to the binding of DDA to the surface of In(0) nanoparticles.[23] The triplet at 2.64 ppm is assigned to –N(CH_2)– bound to In(I)I$(DDA)_x$ and In(III)I_3(DDA) (Figure 7c). Finally, we analyzed the dark-brown solution obtained by mixing 3 eq. of In(I)I, 3 eq. of DDA, and 1 eq. of Sb$(NMe_2)_3$ for 1 h at 50 °C. In the ^{1}H NMR spectrum, a singlet from DMA appears at 2.19 ppm showing that the transamination between Sb$(NMe_2)_3$ and DDA occurred (Figure 7d). The slightly shifted value and broadened signal compared to Figure 7c (2.26 ppm) is possibly due to DMA interacting with different indium species. Interestingly, after only 10 min of premixing, the DMA peak appeared as a singlet at 2.26 ppm indicating that coordination with metal species did not happen at this stage. (Figure S17a, Supporting Information). After 30 min, the dissolution of the In(I) precursor became visible as the initial suspension becomes colored. A broad signal at 2.18 ppm appeared, however, we can still observe a sharp singlet at 2.15 ppm, likely corresponding to an intermediate complex (Figure S17b, Supporting Information). Only after an hour, the broad signal attributed to DMA interacting with both In and Sb becomes uniform. Moreover, the triplet peak of –N(CH_2)– from DDA bound to Sb at 3.73 ppm completely disappeared, which indicates the interaction between Sb and In centers (Figure 7c). At the same time, the signal of –N(CH_2)– observed in the In(I)I-DDA mixture (Figure 7d) is slightly shifted to 2.62 ppm and broadened. We emphasize that when the premixing step is performed at room temperature for 1 h, no changes were observed in the ^{1}H-NMR spectrum of the mixture.

Summarizing, the control experiments and preliminary NMR results presented in this section point toward the existence of an intermediate complex comprising a preformed In–Sb bond. The required experimental conditions for its formation have been determined by exploring the influence of relevant parameters (solvent, mixing time, temperature). We found that the formation of this intermediate complex, whose precise identification necessitates additional studies, is a prerequisite for obtaining high-quality InSb QDs with well-defined absorption features and hence narrow size distributions.

3. Conclusion

NIR/SWIR absorbing colloidal InSb QDs were synthesized using In(I)X (X: Cl, Br, or I) and Sb$(NMe_2)_3$ as precursors. In(I)X acts as a mild reducing agent for Sb$(NMe_2)_3$ being itself oxidized from In(I) to In(III) and serving simultaneously as the indium source. The wavelengths of the excitonic absorption peaks of the resulting InSb QDs could be tuned from 630 to 1880 nm by varying the halide type in the In(I)X precursor, In:Sb ratio, reaction temperature, reaction time, and using for the largest sizes a secondary precursor injection. Concerning the nature of the indium halide, In(I)Cl turned out not suitable to produce QDs with a narrow size distribution unlike In(I)Br and In(I)I. In(I)Br gave access to longer wavelengths (910–1890 nm) while In(I)I covers 630–1350 nm. The difference in the indium–halide bond dissociation energy and the involvement of the halides in the NC surface passivation are at the origin of this behavior. The presented synthesis method gives access to a broad size range of InSb QDs tunable from ≈2 to 7 nm and a comparably narrow size distribution of the as-synthesized samples. The extreme oxophilicity of InSb has become visible in variable-energy X-ray photoelectron spectroscopy analyses. Despite the very short air exposure during the transfer of the samples, a core/shell structure consisting of a pure InSb core and a thin indium oxide shell was obtained. Analysis of the valence band signal indicates that the obtained InSb QDs exhibit an n-type character, which could be either intrinsic or induced by the oxide shell. The premixing step of the In and Sb precursors at 50 °C for at least 1 h turned out mandatory for achieving narrow size distribution. Control reactions and NMR analyses point to the conclusion that molecular species (complexes or clusters) containing preformed In–Sb bonds are generated during the preheating stage as reaction intermediates. Only in this case, the excessive formation of metallic side products such as indium nanoparticles can be avoided and continuous growth from solution be achieved. Summarizing, these results and in particular the broad wavelength tunability suggest that RoHS-compliant InSb QDs are promising candidates for replacing toxic Pb- or Hg-chalcogenide QDs in applications relying on absorption in the NIR/SWIR range.[13] We anticipate that InSb QDs have also a high potential as NIR/SWIR emitters, provided that appropriate core/shell structures can be prepared to passivate effectively the surface and shield the highly oxygen-sensitive surface of InSb from the environment. Protection against oxidation could also be achieved through the passivation with appropriate inorganic surface ligands, as has been shown recently for the case of InAs QDs.[24] These developments pave the way for the use of InSb QDs in NIR/SWIR applications such as photodetectors and cameras, biological detection, telecommunications, and QLEDs.[13b,c,25]

4. Experimental Section

Chemicals: Indium(I) chloride (In(I)Cl, 99.995%) and indium(I) bromide (In(I)Br, 99.998%) were purchased from Alfa-Aesar. Indium(I) iodide (In(I)I, 99999%), tris(dimethylamido)antimony (Sb$(NMe_2)_3$, 99.99%), oleylamine (OAm, ≥98%), dodecylamine (DDA, ≥99.5%), toluene-d_8 (99%), toluene (anhydrous), chloroform (anhydrous), methanol (anhydrous), acetone (anhydrous), and tetrachloroethylene (>99%, anhydrous) were purchased from Aldrich. Tri-n-octylphosphine (TOP, 97%) was purchased from STREM. All chemicals were used without further purification.

Synthesis of InSb QDs using In(I)Cl or In(I)Br and $Sb(NMe_2)_3$ as Precursors: First, 0.17 mmol of $Sb(NMe_2)_3$ was dispersed in 0.4 mL of degassed OAm at 50 °C in a glove box. The $Sb(NMe_2)_3$ was added to 1.0 mmol of In(I)Cl or In(I)Br in 1.6 mL of degassed OAm solution to prepare InSb precursor solution which was stirred for 1 h at 50 °C in a glove box. In a three-necked round-bottom flask (r.b.f), 4 mL of ODE (or OAm) was degassed for l h at 120 °C, then heated to 230 °C under Ar atmosphere. After that, 0.3 mL of TOP and 2 mL of InSb precursor solution were injected into the ODE (or OAm) solvent at 230 °C and the reaction mixture was kept at this temperature and stirred for 3–90 min. The crude material was then purified using the standard procedure (see below).

Synthesis of InSb QDs using In(I)I and $Sb(NMe_2)_3$ as Precursors: The same method as for In(I)Cl or In(I)Br precursors is applied, but using 0.5 mmol of In(I)I.

Heat-Up Synthesis of InSb QDs using In(I)Br and $Sb(NMe_2)_3$ as Precursors: First, 0.17 mmol of $Sb(NMe_2)_3$ was dispersed in 0.4 mL of degassed OAm at 50 °C in a glove box. The $Sb(NMe_2)_3$ was added to 1.0 mmol of In(I)Br in 1.6 mL of degassed OAm solution to prepare InSb precursor solution which was stirred for 1 h at 50 °C in a glove box. In a three-necked r.b.f, 4 mL of ODE (or OAm) was degassed for l h at 120 °C, then cooled down to room temperature under Ar atmosphere. After that, 0.3 mL of TOP and 2 mL of InSb precursor solution were injected into the ODE (or OAm) solvent at room temperature and the reaction mixture was heated to 230 °C with a heating rate of 20–30 °C min^{-1} and stirred for 3–60 min.

Heat-Up Synthesis of InSb QDs using In(I)I and $Sb(NMe_2)_3$ as Precursors: The same method as for In(I)Br precursors is applied, but using 0.5 mmol of In(I)I.

Synthesis of Larger InSb QDs via Secondary Precursor Addition: First, 0.17 mmol of $Sb(NMe_2)_3$ was dispersed in 0.4 mL of degassed OAm at 50 °C in a glove box. The $Sb(NMe_2)_3$ was added to 1.0 mmol of In(I)Br in 1.6 mL of degassed OAm solution to make InSb precursor solution. The stirring of the InSb precursor solution was performed for 1 h at 50 °C in a glove box. In a three-necked r.b.f, 4 mL of ODE was degassed for l h at 120 °C, then heated to 260 °C under Ar atmosphere. After that, 0.3 mL of TOP and 2 mL of InSb precursor solution were injected into the ODE solvent at 260 °C and it was stirred for 60 min. For the second precursor addition, the InSb precursor solution is made again using 0.25 mmol of In(I)Br, and 0.04 mmol of $Sb(NMe_2)_3$ in 0.75 mL of OAm for 1 h at 50 °C. The second precursor solution is injected by a syringe pump with 3 mL h^{-1} of the pumping rate into the InSb QDs solution at 260 °C for 15 min.

Synthesis of InSb QDs Without Premixing of In(I)Br and $Sb(NMe_2)_3$: First, 0.17 mmol of $Sb(NMe_2)_3$ was dispersed in 0.4 mL of degassed OAm at 50 °C in a glove box. In a three-necked round-bottom flask, 1.0 mmol of In(I)Br, 0.3 mL of TOP, and 5.6 mL of degassed OAm were heated to 230 °C under an Ar atmosphere. After that, 0.4 mL of $Sb(NMe_2)_3$–OAm solution was injected into the round-bottom flask containing In(I)Br and it was stirred for 10 min.

Purification of InSb QDs: Inside a glove box, 0.5 mL of the crude sample was centrifuged at 10 000 rpm for 1 min and the greyish precipitate was discarded. The supernatant was mixed with 0.5 mL of anhydrous chloroform, 1.5 ml of anhydrous methanol, and 3 mL of anhydrous acetone. After vortexing, this mixture was centrifuged at 8 000 rpm for 2 min. The obtained black precipitate was redispersed in 0.5 mL of anhydrous tetrachloroethylene for the optical characterizations or in toluene for storage. To eliminate excess organics, the described precipitation/redispersion cycle is repeated.

Characterization: Absorption spectra were measured on a Jasco V-770 UV-vis-NIR spectrometer. The excitonic absorption peak was fitted with a Gaussian function to determine its energy and line width. The emission spectra were obtained using Horiba Fluorolog 3 spectrophotometer equipped with a Hamamatsu R5509 NIR photomultiplier tube. Powder X-ray diffraction patterns were recorded using a Bruker powder diffractometer equipped with a copper anode ($\lambda K_{\alpha 1}$ = 1.5406 Å, $\lambda K_{\alpha 2}$ = 1.5444 Å) and an X'celerator 1D detector. The elemental compositions were analyzed using a Zeiss Ultra 55+ scanning electron microscope equipped with a Bruker QUANTAX energy-dispersive X-ray probe. Transmission electron microscopy was performed by an FEI Tecnai F20 microscope operated at 200 kV. NMR spectra were recorded on a Bruker Avance spectrometer at 400.13 MHz for ^{1}H, and equipped with a 5 mm z-gradient BBO SmartProbe. All measurements were performed at 298 K. The relaxed ^{1}H spectra (recycling time of 5 s) were integrated after baseline correction. The chemical shifts for ^{1}H in toluene-d8 are relative to tetramethylsilane. For the samples in toluene-d8, the CH_3 signal of residual solvent was set at 2.11 ppm in the ^{1}H spectra.

X-Ray Photoemission Measurements (XPS): For photoemission spectroscopy, the Tempo beamline of synchrotron Soleil was used. Films of nanocrystals were spin-casted onto a gold-coated Si substrate (the gold layer was 80 nm thick). The pristine solution of InSb has been used and drop-casted on the substrate within a glove box. The sample is kept under nitrogen atmosphere before its introduction in the ultra-high vacuum photoemission setup. Samples were introduced in the preparation chamber and degassed until a vacuum below 10^{-9} mbar was reached. Then samples were introduced into the analysis chamber. The signal was acquired by a MBS A-1 photoelectron analyzer. The acquisition was carried out at constant pass energy (50 eV) within the detector. Photon energy of 150 eV was used for the acquisition of the valence band while 700 and 1100 eV photon energy was used for the analysis of the core levels The zero binding energy (BE) reference (i.e., the Fermi level) was taken at the leading edge of a clean Au film. The acquired data were processed by subtracting a Shirley/linear background and using Voigt curves for peak fitting.

Supporting Information

Supporting Information is available from the Wiley Online Library or from the author.

Acknowledgements

The authors acknowledge financial support from the French Government within the framework of the Nano2022 (IPCEI Microelectronics) program and the European Union's Horizon research and innovation program under grant agreement 101135704 (HortiQD project). E.L. acknowledges funding via ERC AQDtive (grant 101086358), from Agence Nationale de la recherche (ANR) through the grant Copin (ANR-19-CE24-0022), Frontal (ANR-19-CE09-0017), Bright (ANR-21-CE24-0012), and Quicktera (ANR-22-CE09-0018). The authors thank Stéphanie Pouget for assistance with powder X-ray diffraction.

Conflict of Interest

The authors declare no conflict of interest.

Data Availability Statement

The data that support the findings of this study are available from the corresponding author upon reasonable request.

Keywords

III-V semiconductor nanocrystals, InSb quantum dots, near-infrared (NIR), photodetectors, short-wavelength infrared (SWIR)

Received: March 4, 2024
Revised: May 1, 2024
Published online:

[1] H. Lu, G. M. Carroll, N. R. Neale, M. C. Beard, *ACS Nano* **2019**, *13*, 939.

[2] a) C. Gréboval, A. Chu, N. Goubet, C. Livache, S. Ithurria, E. Lhuillier, *Chem. Rev.* **2021**, *121*, 3627; b) C. Livache, B. Martinez, N. Goubet, J. Ramade, E. Lhuillier, *Frontiers in Chemistry* **2018**, *6*, 575; c) S. B. Hafiz, M. Scimeca, A. Sahu, D.-K. Ko, *Nano Convergence* **2019**, *6*, 7.
[3] a) R. H. Wilson, K. P. Nadeau, F. B. Jaworski, B. J. Tromberg, A. J. Durkin, *J. Biomed. Opt.* **2015**, *20*, 030901; b) S. Chinnathambi, N. Shirahata, *Sci. Technol. Adv. Mater.* **2019**, *20*, 337; c) H. M. Gil, T. W. Price, K. Chelani, J.-S. G. Bouillard, S. D. J. Calaminus, G. J. Stasiuk, *iScience* **2021**, *24*, 102189; d) M. Jiao, A. S. Portniagin, X. Luo, L. Jing, B. Han, A. L. Rogach, *Adv. Opt. Mater.* **2022**, *10*, 2200226.
[4] a) Q. Ma, X. Su, *Analyst* **2010**, *135*, 1867; b) L. Chen, H. Han, *Microchim. Acta* **2014**, *181*, 1485; c) Y. Ma, Y. Zhang, W. W. Yu, *J. Mater. Chem. C* **2019**, *7*, 13662.
[5] Y. Tian, H. Luo, M. Chen, C. Li, S. V. Kershaw, R. Zhang, A. L. Rogach, *Nanoscale* **2023**, *15*, 6476.
[6] L. Börnstein, *Indium antimonide (InSb), energy gap*, (Eds: O. Madelung, U. Rössler, M. Schulz), Springer-Verlag, Berlin Heidelberg **2002**.
[7] A. L. Efros, M. Rosen, *Phys. Rev. B* **1998**, *58*, 7120.
[8] C. M. Evans, S. L. Castro, J. J. Worman, R. P. Raffaelle, *Chem. Mater.* **2008**, *20*, 5727.
[9] A. Maurice, M. L. Haro, B. Hyot, P. Reiss, *Part. Part. Syst. Charact.* **2013**, *30*, 828.
[10] W. Liu, A. Y. Chang, R. D. Schaller, D. V. Talapin, *J. Am. Chem. Soc.* **2012**, *134*, 20258.
[11] T. Zhao, N. Oh, D. Jishkariani, M. Zhang, H. Wang, N. Li, J. D. Lee, C. Zeng, M. Muduli, H.-J. Choi, D. Su, C. B. Murray, C. R. Kagan, *J. Am. Chem. Soc.* **2019**, *141*, 15145.
[12] a) M. Yarema, M. V. Kovalenko, *Chem. Mater.* **2013**, *25*, 1788; b) S. Tamang, K. Kim, H. Choi, Y. Kim, S. Jeong, *Dalton Trans.* **2015**, *44*, 16923; c) R. W. Crisp, G. Grimaldi, L. De Trizio, W. H. Evers, N. Kirkwood, S. Kinge, L. Manna, L. D. A. Siebbeles, A. J. Houtepen, *Nanoscale* **2018**, *10*, 11110; d) S. Busatto, M. de Ruiter, J. T. B. H. Jastrzebski, W. Albrecht, V. Pinchetti, S. Brovelli, S. Bals, M.-E. Moret, C. de Mello Donega, *ACS Nano* **2020**, *14*, 13146.
[13] a) W. J. Mir, T. Sheikh, S. Nematulloev, P. Maity, K. E. Yorov, A.-H. Emwas, M. N. Hedhili, M. S. Khan, M. Abulikemu, O. F. Mohammed, O. M. Bakr, *Small* **2024**, *20*, 2306535; b) Y. Zhang, P. Xia, B. Rehl, D. H. Parmar, D. Choi, M. Imran, Y. Chen, Y. Liu, M. Vafaie, C. Li, O. Atan, J. M. Pina, W. Paritmongkol, L. Levina, O. Voznyy, S. Hoogland, E. H. Sargent, *Angew. Chem., Int. Ed.* **2024**, *63*, 202316733; c) L. Peng, Y. Wang, Y. Ren, Z. Wang, P. Cao, G. Konstantatos, *ACS Nano* **2024**, *18*, 5113.
[14] Muhammad, D. C., D. H. Parmar, B. Rehl, Y. Zhang, O. Atan, G. Kim, P. Xia, J. M. Pina, M. Li, Y. Liu, O. Voznyy, S. Hoogland, E. H. Sargent, *Adv. Mater.* **2023**, *35*, 2306147.
[15] M. Ginterseder, D. Franke, C. F. Perkinson, L. Wang, E. C. Hansen, M. G. Bawendi, *J. Am. Chem. Soc.* **2020**, *142*, 4088.
[16] R. Yadav, Y. Kwon, C. Rivaux, C. Saint-Pierre, W. L. Ling, P. Reiss, *J. Am. Chem. Soc.* **2023**, *145*, 5970.
[17] J. van Embden, A. S. R. Chesman, J. J. Jasieniak, *Chem. Mater.* **2015**, *27*, 2246.
[18] a) Y. Kim, H. Choi, Y. Lee, W.-k. Koh, E. Cho, T. Kim, H. Kim, Y.-H. Kim, H. Y. Jeong, S. Jeong, *Nat. Commun.* **2021**, *12*, 4454; b) Y. Kim, J. H. Chang, H. Choi, Y.-H. Kim, W. K. Bae, S. Jeong, *Chem. Sci.* **2020**, *11*, 913.
[19] a) I. Mohammad, L. Blondeau, E. Foy, J. Leroy, E. Leroy, H. Khodja, M. Gauthier, *Sustainable Energy Fuels* **2021**, *5*, 3825; b) D. Seo, J. Na, S. Lee, S. Lim, *Appl. Surf. Sci.* **2017**, *399*, 523.
[20] a) J. Qu, C. Livache, B. Martinez, C. Gréboval, A. Chu, E. Meriggio, J. Ramade, H. Cruguel, X. Z. Xu, A. Proust, F. Volatron, G. Cabailh, N. Goubet, E. Lhuillier, *ACS Appl. Nano Mater.* **2019**, *2*, 1621; b) B. Tandon, S. A. Shubert-Zuleta, D. J. Milliron, *Chem. Mater.* **2022**, *34*, 777; c) K. Kim, L. C. Reimnitz, S. H. Cho, J. Noh, Z. Dong, S. L. Gibbs, B. A. Korgel, D. J. Milliron, *Chem. Mater.* **2020**, *32*, 9347; d) S. L. Gibbs, C. M. Staller, D. J. Milliron, *Acc. Chem. Res.* **2019**, *52*, 2516.
[21] a) A. Buffard, S. Dreyfuss, B. Nadal, H. Heuclin, X. Xu, G. Patriarche, N. Mézailles, B. Dubertret, *Chem. Mater.* **2016**, *28*, 5925; b) M. D. Tessier, K. De Nolf, D. Dupont, D. Sinnaeve, J. De Roo, Z. Hens, *J. Am. Chem. Soc.* **2016**, *138*, 5923; c) V. Srivastava, E. Dunietz, V. Kamysbayev, J. S. Anderson, D. V. Talapin, *Chem. Mater.* **2018**, *30*, 3623.
[22] M. J. Hostetler, J. E. Wingate, C.-J. Zhong, J. E. Harris, R. W. Vachet, M. R. Clark, J. D. Londono, S. J. Green, J. J. Stokes, G. D. Wignall, G. L. Glish, M. D. Porter, N. D. Evans, R. W. Murray, *Langmuir* **1998**, *14*, 17.
[23] Z. Hens, J. C. Martins, *Chem. Mater.* **2013**, *25*, 1211.
[24] B. K. Jung, H. Yoo, B. Seo, H. J. Choi, Y. K. Choi, T. H. Kim, N. Oh, S. Y. Kim, S. Kim, Y. Lee, J. W. Shim, H. Y. Park, G. W. Hwang, T. N. Ng, S. J. Oh, *ACS Energy Lett.* **2024**, *9*, 504.
[25] T. Kim, D. Shin, M. Kim, H. Kim, E. Cho, M. Choi, J. Kim, E. Jang, S. Jeong, *ACS Energy Lett.* **2023**, *8*, 447.